nature chemical biology

ARTICLES

https://doi.org/10.1038/s41589-018-0193-2

A genetics-free method for high-throughput discovery of cryptic microbial metabolites

Fei Xu[1,3], Yihan Wu[1,3], Chen Zhang[1], Katherine M. Davis[1], Kyuho Moon[1], Leah B. Bushin[1] and Mohammad R. Seyedsayamdost[1,2*]

Bacteria contain an immense untapped trove of novel secondary metabolites in the form of 'silent' biosynthetic gene clusters (BGCs). These can be identified bioinformatically but are not expressed under normal laboratory growth conditions. Methods to access their products would dramatically expand the pool of bioactive compounds. We report a universal high-throughput method for activating silent BGCs in diverse microorganisms. Our approach relies on elicitor screening to induce the secondary metabolome of a given strain and imaging mass spectrometry to visualize the resulting metabolomes in response to ~500 conditions. Because it does not require challenging genetic, cloning, or culturing procedures, this method can be used with both sequenced and unsequenced bacteria. We demonstrate the power of the approach by applying it to diverse bacteria and report the discovery of nine cryptic metabolites with potentially therapeutic bioactivities, including a new glycopeptide chemotype with potent inhibitory activity against a pathogenic virus.

Modern medicine is unimaginable without natural products. Predominantly isolated from microorganisms and plants, these molecules, also referred to as secondary metabolites, form the basis of >70% of antibiotics, >50% of anticancer agents, and overall more than half of the drugs approved in the United States in the past 35 years (refs. [1–3]). After nearly a century of mining for secondary metabolites, microorganisms appeared to have become an exhausted resource. However, the recent explosion in microbial genome sequences suggests a massive untapped trove of new metabolites[4–9]. Specifically, members of several bacterial phyla typically contain 25 or more BGCs—sets of genes that direct the biosynthesis of a natural product—that are not actively, or are only weakly, expressed under standard laboratory conditions. These so-called 'silent' or 'cryptic' BGCs outnumber the constitutively active ones by a factor of 5–10. As such, finding new methods that access their products could substantially enhance the repertoire of novel natural products and thereby accelerate and facilitate drug discovery.

The importance of inducing silent BGCs has been recognized by the research community, and several approaches have been developed to identify and characterize their small-molecule products, including expression of BGCs in a heterologous host, coculture screening, ribosome engineering, insertion of constitutive or inducible promoters, reporter-guided mutant selection, and endogenous overexpression of regulatory proteins[9–17]. We have added to this canon of approaches by developing high-throughput elicitor screening (HiTES)[18–20], a strategy that identifies small-molecule elicitors for a given silent BGC. Although these methods have collectively begun to illuminate the hidden secondary metabolomes of bacteria, they typically necessitate challenging culturing conditions (i.e., cocultures or mixed cultures), molecular biology procedures, and/or genetic manipulations, which slow the pace and throughput of natural-product discovery. A definitive method for accessing cryptic metabolites in varied microorganisms has yet to be developed.

Herein, we work toward that goal and report a genetics-free endogenous monoculture strategy for eliciting and detecting the cryptic secondary metabolomes of diverse bacteria. We use HiTES in conjunction with imaging mass spectrometry (IMS), a method that we refer to as HiTES–IMS, to induce silent BGCs and to detect the resulting small molecules in a rapid and untargeted fashion. Computational methods are then employed to identify the desired cryptic metabolites as well as their elicitors. Rather than monitor one silent BGC at a time, HiTES–IMS enables interrogation of the global secondary metabolome of any culturable bacterium in response to 500–1,000 conditions. Application of this approach in Gram-negative and Gram-positive bacteria uncovered nine cryptic metabolites, including a new post-translationally modified lasso peptide as well as a new glycopeptide chemotype that, in in vitro assays, is more potent than the currently used drug against the respiratory syncytial virus (RSV). Our approach is widely applicable to sequenced and unsequenced bacteria or bacterial consortia, and it holds promise in unearthing the vast hidden metabolomes of microorganisms and expediting the search for new therapeutic agents from microbial sources.

Results

Replacing genetics with imaging mass spectrometry. The HiTES approach consists of two components: the activation of silent or weakly expressed BGCs by elicitor screening and a readout for this process, which to date has relied on genetic reporter assays[18,19]. The detection step limits the throughput of HiTES, because creating the appropriate genetic constructs is often time consuming, if not impossible, depending on the strain. In addressing this drawback, we were inspired by recent advances in MS technologies[21] and sought to replace genetic reporter assays with IMS as a readout for secondary-metabolite production. We envisioned a workflow consisting of subjecting the wild-type microorganism to elicitor screening, then imaging the resulting 500–1,000 metabolomes, as a function of each molecule in the library, by using IMS (Fig. 1). Computational approaches and appropriate visualization would then be used to pinpoint cryptic metabolites.

To implement this idea, we selected orfamides as a test case. Orfamides are sparingly produced metabolites isolated from

[1]Department of Chemistry, Princeton University, Princeton, NJ, USA. [2]Department of Molecular Biology, Princeton University, Princeton, NJ, USA. [3]These authors contributed equally: Fei Xu, Yihan Wu. *e-mail: mrseyed@princeton.edu

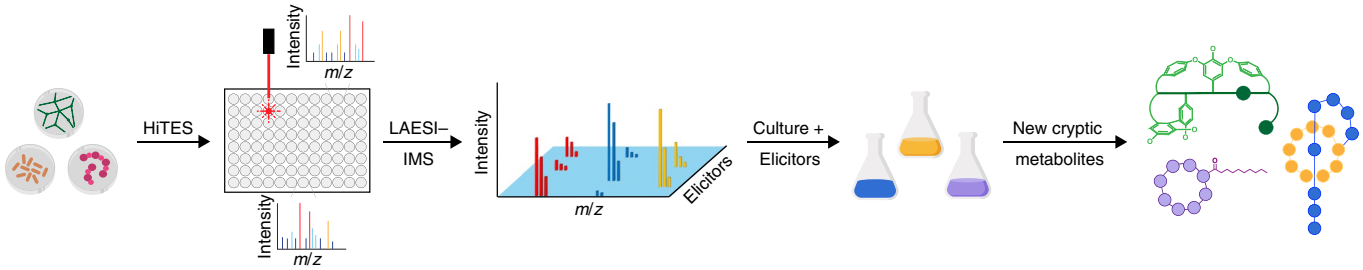

Fig. 1 | HiTES–IMS workflow. A bacterial culture is arrayed into 96-well plates and subjected to high-throughput elicitor screening. After a suitable incubation period, the cultures are assessed by LAESI–IMS in 96-well format. The observed global metabolome is depicted in a 3D plot that links each elicitor to metabolites, characterized by their *m/z* and MS intensity values. Large-scale cultures with the appropriate elicitor facilitate isolation and characterization of new cryptic metabolites.

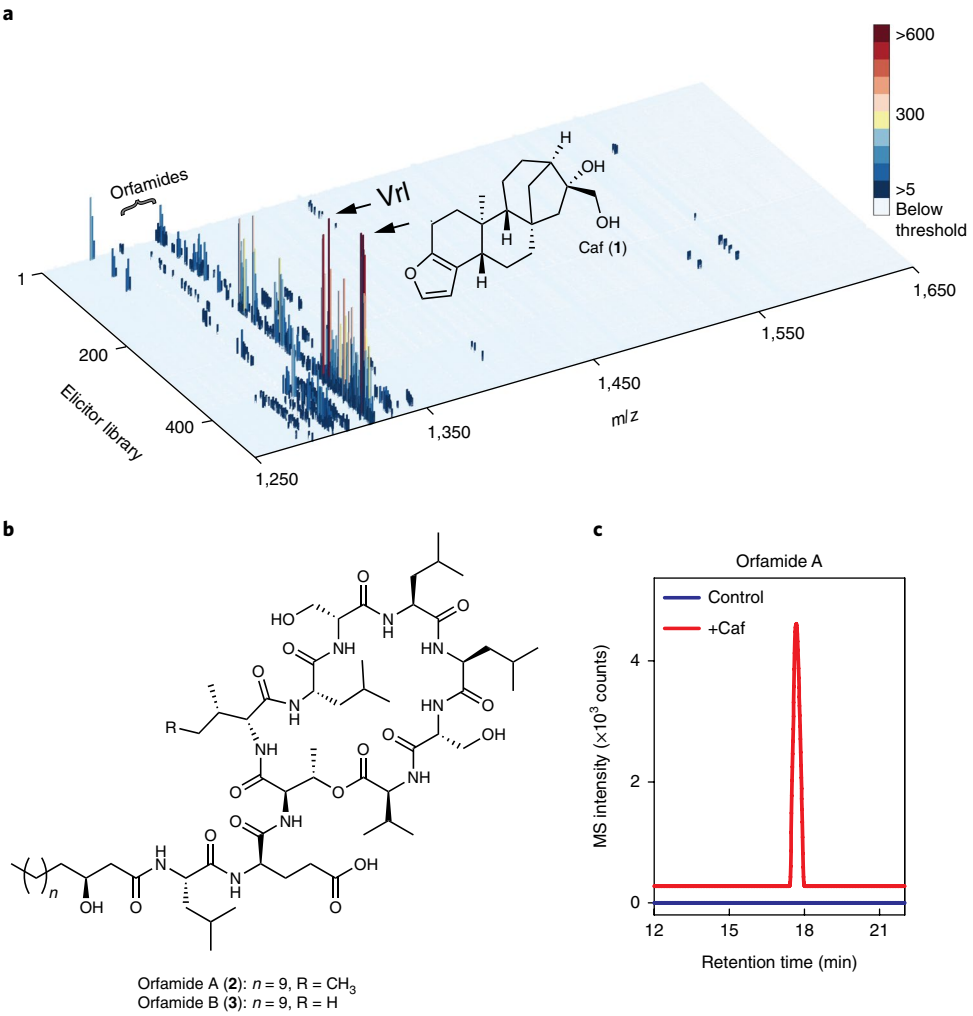

Fig. 2 | Proof-of-concept application of HiTES–IMS to *P. protegens*. **a**, 3D plot relating the *P. protegens* metabolome, in terms of *m/z* and MS intensity, to each elicitor. MS data were collected in the *m/z* range of 1,200–2,000 to focus on orfamide production, in response to a 502-member natural-product library. No signals were detected below *m/z* 1,250 or above *m/z* 1,650. MS intensity (in counts) is color-coded according to the color bar shown. 'Below threshold' indicates signals below the five-count threshold, which were therefore not included in the plot. Orfamides are labeled, as are the best elicitors of orfamide synthesis, cafestol (Caf) and vinorelbine (Vrl). **b**, Structures of orfamide A and B. **c**, Validation of cafestol as an inducer of orfamide A in flask cultures analyzed by HPLC–MS. Shown are HR–MS extracted ion chromatograms of orfamide A from untreated (blue) and cafestol-treated (red) cultures. The HiTES–IMS screen was carried out in a single replicate; production of desired metabolites was validated in three independent biological replicates; a representative result is shown in **c**. All three replicates yielded similar levels of induction of orfamides.

Pseudomonas protegens Pf-5 (hereafter denoted *P. protegens*). A genome-isotopic approach was previously used to identify these compounds and ultimately to solve their structures[22]. As a proof of concept for our strategy, wild-type *P. protegens* was cultured in 96-well plates and subjected to HiTES with a 502-member natural-product library. We analyzed the resulting metabolomes with

laser-ablation-coupled electrospray ionization MS (LAESI–MS), an emerging method in which a midinfrared laser ($\lambda = 2.94\,\mu m$) is absorbed by the sample, thus generating an ablation plume of neutral metabolites that are ionized via electrospray and introduced into the mass spectrometer[23–26]. LAESI–IMS combines a soft ionization method with broad molecular coverage—including peptides, lipids, and alkaloids among others—with detection sensitivities in the single-digit micromolar range for many types of metabolites[26]. Compared with other IMS methods, LAESI–IMS is advantageous because it can be applied to liquid or solid surfaces and live bacterial cultures with minimal sample preparation at ambient pressure. It shares with other IMS techniques the disadvantage of ion suppression and preferential detection of more ionizable metabolites. The optimization of numerous parameters (Methods) facilitated rapid characterization of the *P. protegens* metabolome within each of the 502 wells, thus allowing us to image a 96-well-plate liquid culture in less than an hour. The signals observed in each well above a set cutoff value were computationally extracted and amalgamated into a 3D plot depicting the intensity and *m*/*z* for each metabolite produced in the presence of a given elicitor (Fig. 2a and Supplementary Fig. 1). By visually inspecting the 502 metabolomes represented in the 3D plot, we were easily able to detect induction of orfamides—specifically analogs A (**2**) and B (**3**), and several unknown derivatives—to varying degrees (Fig. 2a,b). Optimal production was triggered by the mild cytotoxin cafestol (**1**) and the anticancer agent vinorelbine, compounds previously not known to elicit secondary metabolism. Cafestol's stimulatory activity was further confirmed with HPLC–MS, thus validating the use of HiTES–IMS in inducing silent or weakly expressed BGCs (Fig. 2c and Supplementary Table 1). The simplicity of this approach suggested that it could be broadly applied.

Application of HiTES–IMS to streptomycetes. After the success in *P. protegens*, we next applied HiTES–IMS to *Streptomyces* spp., the most prolific genus of bacterial secondary-metabolite producers known. We chose *Streptomyces canus* NRRL B3980, which is related to the amphomycin producer and contains more than 20 BGCs that have not been linked to a natural product[27,28]. The results of HiTES–IMS with *S. canus*, again with a 502-member natural-product library, are shown in 3D representation (Fig. 3a and Supplementary Fig. 2). Several metabolites were induced in the *m*/*z* range of 250–650 (Supplementary Fig. 2). To optimize our chances of finding new metabolites, we focused on compounds with higher molecular weights (Fig. 3a). In this range, three clusters of peaks, representing three compound families, appeared to be elicited: we detected compounds with *m*/*z* 1,260–1,295, which were identified as the amphomycins in further analysis. The best elicitors for the amphomycins were the flavonol morin and the antimalarial quinine. A second set of induced compounds was also detected with *m*/*z* 1,220–1,245. Finally, we observed induction of a third compound family distinct from the other two, with *m*/*z* of 1,563 and 1,579, elicited by the cyclin-dependent kinase inhibitor kenpaullone (**4**) (Fig. 3a,b). These findings highlight the ability of our approach to induce multiple cryptic BGCs in a parallel fashion. Whereas in our previous renditions of HiTES, we monitored the expression of only a single BGC at a time, the current approach allowed us to monitor all BGCs that could be captured by our detection method in one experiment.

Among the cryptic metabolites elicited, we focused further efforts on the compounds with *m*/*z* 1,579 and 1,563, to which we assigned the trivial names canucin A and B, respectively (Supplementary Table 1). We validated the results observed in 96-well plates and found strong induction of both compounds by kenpaullone (approximately 12-fold in 96-well plates and flask cultures), in agreement with the screening results (Fig. 3c). Large-scale production cultures with kenpaullone as an inducer allowed us to isolate sufficient material

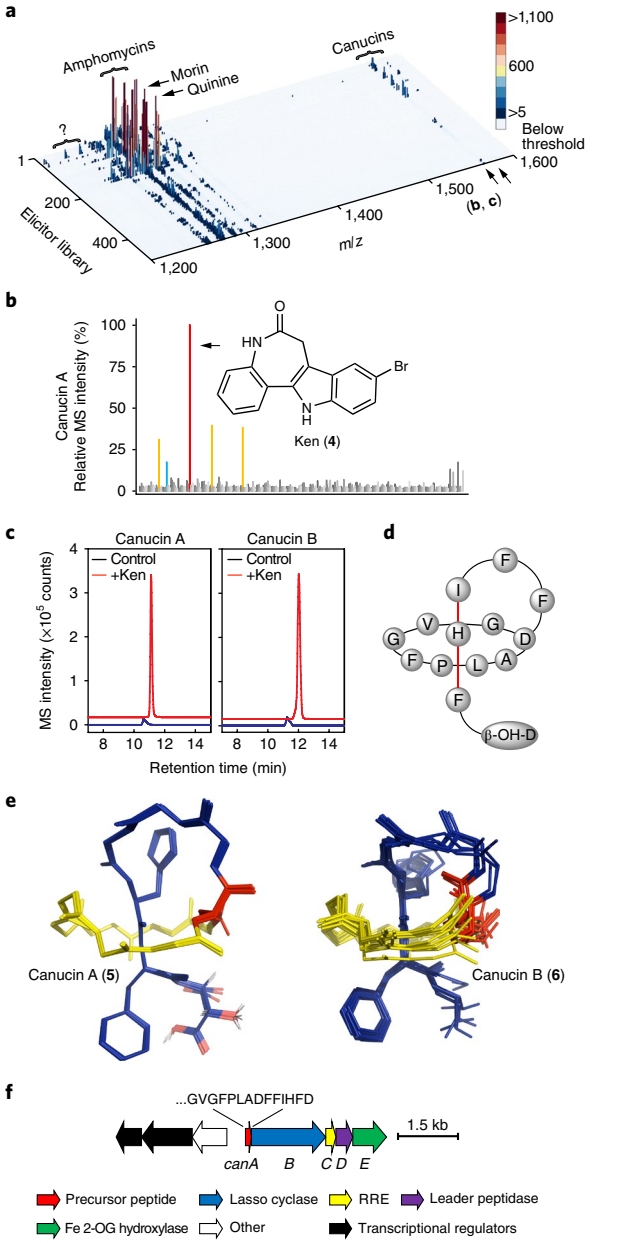

Fig. 3 | Discovery of a novel cryptic lasso peptide by HiTES–IMS. **a**, Secondary metabolome of *S. canus* in response to 502 elicitors. MS data were collected in the *m*/*z* range of 250–1,600 (Supplementary Fig. 2). The high *m*/*z* range is shown to focus on canucins. 'Below threshold' on the color bar (in counts) indicates below the threshold of detection. Morin and quinine, which induce amphomycin synthesis, are marked. Canucins and an uncharacterized set of induced metabolites (question mark) are indicated. **b**, 2D component of the 3D plot focusing on canucin A (*m*/*z* 1579). Kenpaullone (Ken) was the most effective elicitor. **c**, Induction of canucin A and B by kenpaullone in flask cultures analyzed by HPLC–MS. The HR-MS extracted ion chromatogram traces are offset in the *x* and *y* axes for clarity. **d**, Illustration of the topology of canucin A, with His12 and Phe13 providing steric locks. **e**, Overlay of the top-ten computed structures for canucin A and B, obtained from NMR NOESY constraints and the CYANA algorithm. Both exhibit a lasso topology. **f**, BGC for canucins (*can*), as identified by bioinformatic studies. The C-terminal sequence of CanA is shown, along with predicted functions of the tailoring enzymes. The HiTES–IMS screen was carried out in a single replicate; production of desired metabolites was validated in three independent biological replicates, and representative results are shown in **c**. All three replicates yielded similar levels of induction of canucins.

to solve the structures of canucins by 1D/2D NMR. Analysis of ^{1}H, gCOSY and TOCSY NMR data showed that canucin A (**5**) is a peptide with 14 recognizable α-^{1}Hs. HSQC and HMBC analysis revealed that 13 of these were canonical amino acids, whereas one was the modified β-hydroxy-aspartate (Supplementary Table 2 and Supplementary Fig. 3). Further analysis by NMR and HR–MS suggested that canucin A contained an isopeptide bond between residues Gly1 and Asp8, a feature typical of lasso peptides[29,30]. Indeed, NOESY correlations between the C-terminal-tail residues and those surrounding the isopeptide bond suggested that canucin A contains a lasso topology (Supplementary Fig. 3). To verify these results, we collected high-resolution NOESY spectra with various mixing times and solved the 3D structure of canucin A by using the CYANA algorithm, which uses molecular dynamics simulations in a peptide's torsion-angle space to compute the structures that best agree with the NOESY data[31,32]. The ten best structures converged on a lasso topology, in which His12 and Phe13 provide steric locks above and below the ring, respectively (Fig. 3d,e). At 14 amino acids, canucin A is one of the smallest lasso peptides discovered to date.

Repeated efforts to determine the stereochemistry at the β-carbon of the C-terminal aspartate residue through Mosher analysis failed, possibly because of steric hindrance. We subsequently used CYANA to calculate which stereoisomer best fit the observed NOESY correlations. The *S* stereoisomer gave a lower *f* function, a result indicative of a better match between the calculated structure and the set of constraints, as well as a lower backbone r.m.s. deviation (Supplementary Table 3). We suggest that the *S* configuration is present at the β-carbon of aspartate, a prediction to be tested by future experiments. We also identified a second analog, canucin B (**6**). Structural elucidation by HR–MS and NMR identified it as the des-hydroxy variant of canucin A (Supplementary Tables 1 and 4). CYANA calculations confirmed that canucin B contains a lasso topology, again revealing that His12 and Phe13 are steric locks in a topology akin to that of canucin A (Fig. 3e). These results suggest that hydroxylation at the C-terminal aspartate in canucin A occurs after the threaded lasso motif has been installed, although the order remains to be determined experimentally.

Post-translationally modified lasso peptides are rare, and a β-hydroxylated amino acid has not previously been observed within this compound family[29,30,33,34]. To gain insights into the biosynthesis of canucin A, we examined the genome sequence of *S. canus*. We identified a BGC, which we annotate as *can*, with a typical lasso-peptide synteny and a precursor peptide whose C-terminal sequence perfectly matches that of the canucins (Fig. 3f). Aside from the precursor peptide, the *can* BGC contains a typical protease and an asparagine synthetase, which removes the precursor peptide and forms the threaded-lasso motif, respectively[29,30]. In addition, we annotated *canE*, encoding a putative α-ketoglutarate-dependent mononuclear iron enzyme, members of which have been shown to hydroxylate unactivated carbon positions[35,36] (Supplementary Table 5). CanE is likely to be involved in the synthesis of β-OH-aspartate. The discovery of canucins shows that HiTES–IMS can be applied to streptomycetes to unveil new cryptic metabolites.

Application of HiTES–IMS to rare actinomycetes. With the success of HiTES–IMS with common prolific Gram-negative and Gram-positive bacteria, we next sought to apply this approach to rare actinomycetes, a group of bacteria that account for some structurally fascinating and functionally potent metabolites, including the antibiotic of last resort vancomycin as well as the anticancer agent calicheamicin[37–40]. Rare actinomycetes are ideal test cases for HiTES–IMS because, in addition to harboring an abundance of silent BGCs, they are difficult to manipulate genetically, thus all but precluding transcriptional reporter assays. To apply HiTES–IMS, we chose *Amycolatopsis keratiniphila* NRRL B24117 as a test case. Its genome has not been sequenced, but efforts to find further BGCs that encode glycopeptide antibiotics (GPAs) through PCR have shown that it contains a vancomycin-like BGC, although a product has not yet been reported[41]. We subjected *A. keratiniphila* to HiTES–IMS and observed numerous induced metabolites in both low and high *m/z* ranges (Fig. 4a and Supplementary Fig. 4), thus suggesting that this strain possesses a substantial hidden metabolome. Again, induction of silent BGCs occurred in a high-throughput fashion. In the *m/z* range typical for GPAs, a compound with *m/z* 1,286 was induced by galangin and the indole-containing alkaloids evodiamine and ajmaline. Additionally, a compound with *m/z* 1,425 was induced by similar elicitors, including galangin and evodiamine (Supplementary Fig. 4). Finally, compounds with *m/z* 1,654 and 1,811 were observed in the induced metabolome, primarily by dihydroergocristine (Dhe, **7**) and vincamine (Vin, **8**; Fig. 4a,b). *A. keratiniphila* appeared to respond to indole-bearing alkaloids of diverse origins by activating numerous, otherwise silent BGCs, thus leading to the production of cryptic metabolites.

Of the compounds detected, one with *m/z* 1,811 appeared to contain a chlorine atom, as judged by the HR–MS isotope distribution pattern, a common modification in GPAs (Supplementary Table 1). Follow-up experiments validated the strong stimulatory activity by Dhe and Vin, demonstrating a marked elicitation of this metabolite (15-fold in 96-well plates and fourfold in flask cultures with Dhe; Fig. 4c), a finding consistent with the HiTES–IMS screening results. Suspecting that it might be the putative glycopeptide, we isolated seven analogs from large-scale production cultures in the presence of Dhe. HR–MS analysis suggested that these compounds fell into two families: one that we refer to as keratinimicins and a second, the keratinicyclins. 1D/2D NMR analysis showed that keratinimicin A (**9**) contains seven highly modified amino acids, with recognizable α-^{1}Hs at 4.41, 4.45, 4.52, 5.62, 4.23, 4.48, and 4.42 p.p.m. (Fig. 4d and Supplementary Table 6). TOCSY, HSQC, and HMBC analysis identified these as the 3-Cl derivative of 4-hydroxyphenylglycine (Hpg), β-OH-tyrosine, phenylalanine, two cross-linked Hpg residues, a glycosylated β-OH-3-Cl-tyrosine, and a cross-linked 3,5-dihydroxyphenylglycine (Dpg) (Supplementary Fig. 5). Characteristically, the cross-links occurred between rings A and B, via a carbon-carbon bond, and between rings C and D, and D and E, via aryl ether bonds, as elucidated by HMBC and ROESY spectra (Fig. 4e). Four glycosyl groups were identified by NMR analysis: mannose, actinosamine, and a glucose–rhamnose disaccharide on

Fig. 4 | Induction of novel glycopeptides by using HiTES–IMS. a, Secondary metabolome of *A. keratiniphila* in response to 502 elicitors. MS data were collected in the *m/z* range of 250–2,000 (Supplementary Fig. 4). A magnified view is shown to focus on glycopeptides. 'Below threshold' indicates below MS detection threshold. Keratinimicins, keratinicyclins, and uncharacterized induced metabolites (question mark) are indicated. **b**, 2D component of the 3D plot focusing on keratinimicin A (*m/z* 1,811). Dhe and Vin were the most effective elicitors. **c**, Validation of Dhe and Vin as elicitors of keratinimicin and keratinicylin in 96-well cultures analyzed by HPLC–MS. Shown are HR–MS extracted ion chromatograms from untreated (black), Vin-treated (blue), and Dhe-treated (red) cultures. The traces are offset in the *x* and *y* axes for clarity. **d**, Relevant NMR correlations used to solve the structures of keratinimicin A and keratinicyclin A. **e**, Structures of four keratinimicin and three keratinicyclin derivatives with varying substitution patterns. The nomenclature to identify different rings in glycopeptides is shown in keratinimicin A. **f**, The *ker* BGC, as identified by bioinformatic analysis after sequencing the genome of *A. keratiniphila*. The predicted domain composition for each NRPS is shown, as are the predicted functions of the remaining enzymes in the BGC. Tyr* denotes modified tyrosine. The HiTES–IMS screen was carried out in a single replicate; production of desired metabolites was validated in three independent biological replicates; representative results are shown in **c**. All three replicates yielded similar levels of induction of keratinimicins and keratinicyclins.

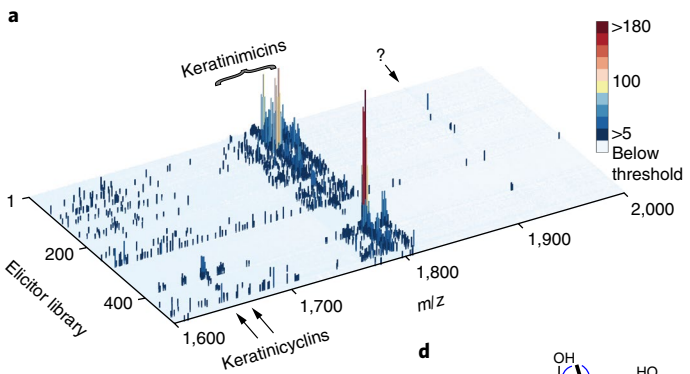
a
Keratinimicins
?
>180
100
>5
Below threshold
1
200
400
Elicitor library
1,600
1,700
1,800
1,900
2,000
m/z
Keratinicyclins

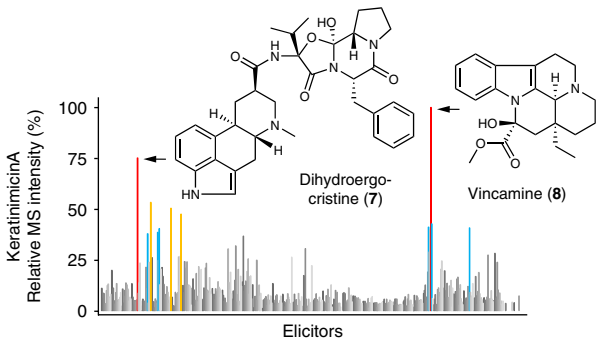
b
KeratinimicinA Relative MS intensity (%)
100
75
50
25
0
Dihydroergo-cristine (7)
Vincamine (8)
Elicitors

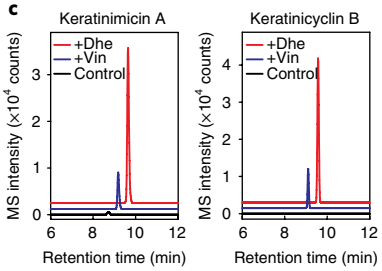
c
Keratinimicin A
Keratinicyclin B
+Dhe
+Vin
Control
MS intensity (×10^4 counts)
Retention time (min)

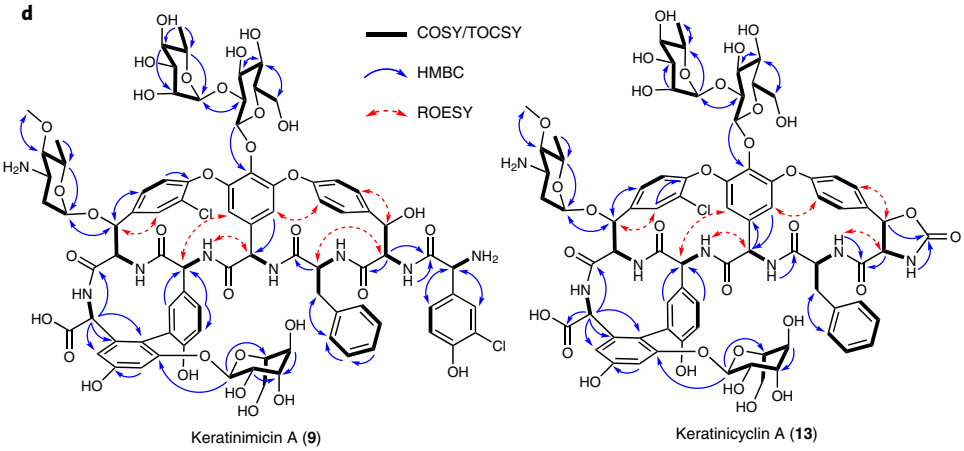
d
COSY/TOCSY
HMBC
ROESY
Keratinimicin A (9)
Keratinicyclin A (13)

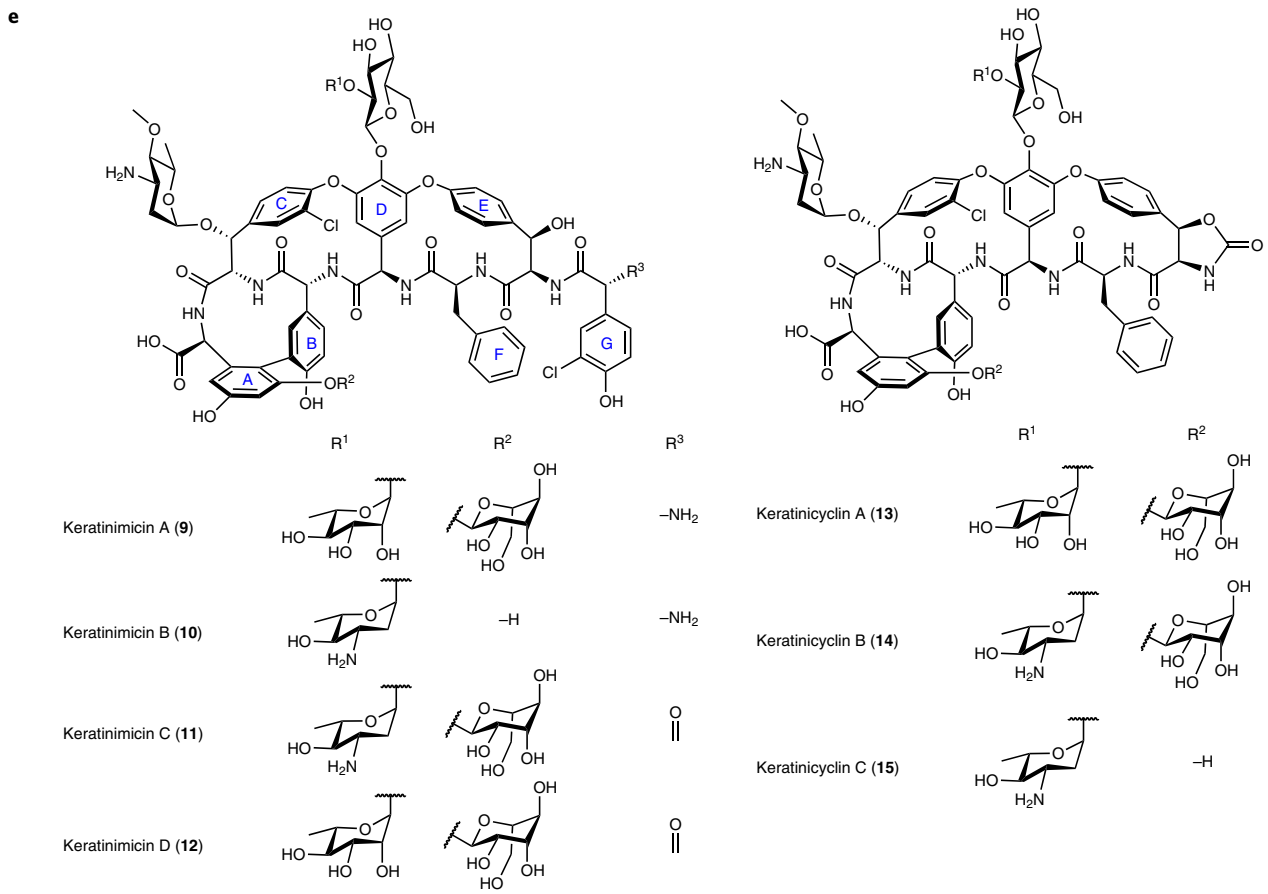
e
R1
R2
R3
Keratinimicin A (9)
Keratinimicin B (10)
Keratinimicin C (11)
Keratinimicin D (12)
Keratinicyclin A (13)
Keratinicyclin B (14)
Keratinicyclin C (15)

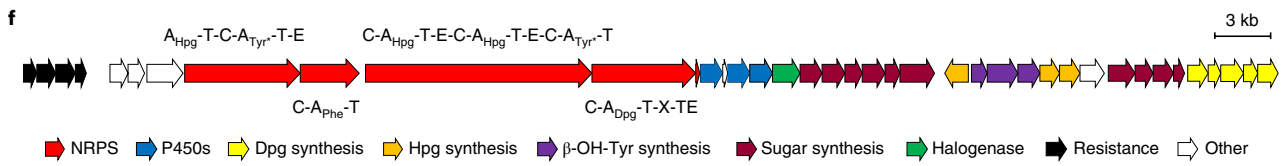
f
3 kb
NRPS
P450s
Dpg synthesis
Hpg synthesis
β-OH-Tyr synthesis
Sugar synthesis
Halogenase
Resistance
Other

Table 1 | MIC values for keratinimicins and keratinicyclin B against select pathogenic Gram-positive bacteria and viruses[a]

Strain	Keratinimicin A	Keratinimicin C	Keratinicyclin B	Control drug[b]
Staphylococcus aureus	4.4	4.5	>39	2.1 (V), 1.5 (C)
Staphylococcus aureus MRSA	2.2	4.5	>39	0.7 (V), 12.1 (C)
Streptococcus pneumoniae PSPP	0.1	0.6	19.5	0.4 (V), 1.5 (C)
Streptococcus pyogenes	0.3	1.1	19.5	0.2 (V), 0.8 (C)
Streptococcus agalactiae	0.6	2.2	39	0.2 (V), 0.8 (C)
Enterococcus faecalis VSE	2.2	4.5	>39	2.8 (V), 6.0 (C)
Enterococcus faecalis VRE	>35	>35	>39	>44 (V), >12.1 (C)
Bacillus subtilis	0.3	1.1	19.5	0.1 (V), 0.2 (C)
Clostridium difficile	0.3	0.3	9.8	1.5 (M)
Influenza A	–[c]	–	92	0.7 (O)
Respiratory syncytial virus	–	–	0.4	7.8 (R)

[a]Values are in micromolar; additional details can be found in Methods and Supplementary Table 14. [b]Control drugs are abbreviated as follows: V, vancomycin; C, ciprofloxacin, M, metronidazole; O, oseltamivir; R, ribavirin. [c]Not determined.

rings A, C, and D, respectively, thus completing the 2D structure of keratinimicin A (Supplementary Fig. 5 and Supplementary Table 6). To assign the chiral centers, we chose a combined spectroscopic and bioinformatic approach. Shotgun sequencing of the entire genome of *A. keratiniphila* allowed us to pinpoint a GPA cluster, which we annotated as *ker*, on the basis of the canonical synteny previously described[39] (Fig. 4f). To the best of our knowledge, *ker* is the first BGC reported for a class II GPA. Bioinformatic analysis revealed a domain organization identical to that of the archetypal class I GPAs (Supplementary Table 7). We therefore propose a pattern of D- and L-amino acids[38] (as shown from C- to N termini: L-L-D-D-L-D-D; Fig. 4e). With this pattern in mind, we tentatively assigned the *R* configuration for the β-OH groups on the basis of NMR ROESY correlations, thus completing the proposed 3D structure. Keratinimicin A is similar to the actinoidins, notably actinoidin B, except that it carries a different disaccharide at residue D[42,43].

Three additional keratinimicin analogs were identified and structurally elucidated. Relative to variant A, keratinimicin B (**10**) contains only three glycosyl moieties: actinosamine and a glucose–acosamine disaccharide on rings C and D, respectively, whereas mannose on ring A is missing (Supplementary Table 8). Keratinimicin C (**11**) is N-terminally capped by an unusual *m*-chloro-*p*-hydroxyphenylglyoxylic acid moiety, again with a different bouquet of sugar substituents (Supplementary Table 9). Keratinimicin D (**12**) also contains the *m*-chloro-*p*-hydroxyphenylglyoxylic acid residue, with yet a different combination of sugars on ring D, relative to keratinimicin C (Supplementary Table 10).

The structure of keratinicyclin A (**13**) was characterized by extensive analysis of spectroscopic data leading to the structure shown (Fig. 4d,e). It consists of a hexamer peptidic backbone containing the same sequence as the keratinimicins but without the N-terminal 3-Cl-Hpg residue. It bears the same aromatic cross-links as the keratinimicins, with an A–B biaryl bond as well as the C-*O*-D and D-*O*-E aryl ether cross-links. The glycosyl groups were also identified by NMR analysis as described above (Supplementary Table 11 and Supplementary Fig. 6). Most notably, the keratinicyclins contain an N-terminal 2-oxazolidinone, a functional group present in the clinically used antibiotics linezolid and tedizolid[44]. Thus, the keratinicyclins combine the characteristic features of the GPAs with those of the oxazolidinone antibiotics, the first such combination reported to date. Within the GPAs, the keratinicyclins represent a new chemotype.

We solved the structures of two additional keratinicyclins. Relative to derivative A, keratinicyclin B (**14**) contains a glucose–acosamine disaccharide on ring D rather than glucose–rhamnose (Supplementary Table 12). Keratinicyclin C (**15**) also contains a glucose–acosamine disaccharide on ring D but lacks mannose on ring A (Supplementary Table 13).

Initial in-house assays revealed strong antimicrobial activity for the keratinimicins but not for the keratinicyclins. Keratinimicins A and C were subjected to broad bioactivity tests against bacterial pathogens. Because some GPAs have been documented to contain antiviral properties[38], keratinicyclin B was assessed against a panel of pathogenic human viruses. Keratinimicins showed potent antibacterial activity against numerous Gram-positive pathogens, with minimal inhibitory concentrations (MICs) akin to those of vancomycin against streptococci, *Clostridium difficile*, and *Enterococcus faecalis* (Table 1 and Supplementary Table 14). They were ineffective against vancomycin-resistant enterococci, thus suggesting that they may have a similar mode of action to that of vancomycin. Keratinicyclin B did not exhibit notable antibacterial activity but was a potent inhibitor against RSV. Indeed, the MIC determined against RSV was ~20-fold more potent than that of the currently used drug, ribavirin[45] (Table 1). The discoveries of these cryptic antibacterial and antiviral agents highlight the utility of HiTES–IMS in unearthing novel metabolites with potentially therapeutic bioactivities.

Discussion

Silent BGCs are a treasure trove of potential new secondary metabolites. Advances in DNA technology and extensive genome sequencing have compiled a massive genome database, which must be mined to harvest the fruits of decades of innovation. The ideal method to do so is one that does not necessitate challenging genetic or cloning procedures of the typically large BGCs. Moreover, the method should activate silent BGCs in a high-throughput fashion, preferably in an endogenous host, to avoid the difficulties associated with heterologous expression. Finally, a monoculture approach is preferred to eliminate the possibility of irreproducible interactions that sometimes plague mixed-culture or coculture screens. Herein, we implemented HiTES–IMS, a method that satisfies all these criteria. We highlighted its utility by applying it to sequenced and unsequenced bacteria, notably a rare actinomycete, a class whose members are difficult to manipulate genetically. The typical output provides a picture of the secondary metabolome of a given bacterium in response to ~500 conditions, thus demonstrating activation of silent BGCs in a high-throughput fashion. Leveraging these advantages, we report a lasso peptide with an unprecedented post-translational modification, new glycopeptide antibiotics with bioactivities similar to or better than that of

vancomycin, and a novel glycopeptide chemotype, which combines features of the GPAs with those of the oxazolidinone antibiotics and exhibits better antiviral activity in vitro than ribavarin, the currently used drug against RSV.

HiTES–IMS adds to the cadre of available approaches for imaging bacterial metabolomes. MALDI–TOF- and DESI-based IMS have been pioneered for assessing bacterial cultures and interspecies interactions[21,46–48]. LAESI–IMS has been used for spatially resolving secondary-metabolite production and for strain selection[23,24,49]. High-throughput elicitation has previously been reported in a compound- and cluster-specific manner along with ion-mobility UPLC–MS to assess a small number of eliciting conditions[18,50,51]. By combining two overarching methods, high-throughput elicitation and IMS, HiTES–IMS facilitates interrogation of cryptic bacterial metabolomes in response to hundreds of conditions.

In contrast to primary metabolism, the complete secondary metabolome of any given prolific bacterium is not yet known[7,52]. Thus, in addition to unearthing novel cryptic metabolites, we propose that HiTES–IMS may be used to uncover global secondary metabolomes, that is, the full biosynthetic capability of selected bacterial species, as detected by MS. Although such discovery was theoretically possible with previous renditions of HiTES and other methods, the advantage of the current approach, and of IMS in general, is that the final product of a BGC, the secondary metabolite, provides the readout, rather than transcriptional or translational assays. Additionally, through linking new cryptic metabolites to an elicitor, the mechanism of elicitation may be investigated, which in turn can lead to the identification of regulatory circuits that kick-start secondary metabolism in response to subinhibitory concentrations of toxins[53–55]. HiTES–IMS is the most general approach to date for activation of silent BGCs, and it is poised to simultaneously shed light onto the products and regulation of cryptic metabolism in diverse bacteria.

Online content

Any methods, additional references, Nature Research reporting summaries, source data, statements of data availability and associated accession codes are available at https://doi.org/10.1038/s41589-018-0193-2.

Received: 17 May 2018; Accepted: 9 November 2018;
Published online: 7 January 2019

References

1. Newman, D. J. & Cragg, G. M. Natural products as sources of new drugs from 1981 to 2014. *J. Nat. Prod.* **79**, 629–661 (2016).
2. Cragg, G. M. & Newman, D. J. Natural products: a continuing source of novel drug leads. *Biochim. Biophys. Acta* **1830**, 3670–3695 (2013).
3. Cragg, G. M., Grothaus, P. G. & Newman, D. J. Impact of natural products on developing new anti-cancer agents. *Chem. Rev.* **109**, 3012–3043 (2009).
4. Bentley, S. D. et al. Complete genome sequence of the model actinomycete *Streptomyces coelicolor* A3(2). *Nature* **417**, 141–147 (2002).
5. Ikeda, H. et al. Complete genome sequence and comparative analysis of the industrial microorganism *Streptomyces avermitilis*. *Nat. Biotechnol.* **21**, 526–531 (2003).
6. Oliynyk, M. et al. Complete genome sequence of the erythromycin-producing bacterium *Saccharopolyspora erythraea* NRRL23338. *Nat. Biotechnol.* **25**, 447–453 (2007).
7. Nett, M., Ikeda, H. & Moore, B. S. Genomic basis for natural product biosynthetic diversity in the actinomycetes. *Nat. Prod. Rep.* **26**, 1362–1384 (2009).
8. Liu, X. & Cheng, Y. Q. Genome-guided discovery of diverse natural products from *Burkholderia* sp. *J. Ind. Microbiol. Biotechnol.* **41**, 275–284 (2014).
9. Baltz, R. H. Gifted microbes for genome mining and natural product discovery. *J. Ind. Microbiol. Biotechnol.* **44**, 573–588 (2017).
10. Okada, B. K. & Seyedsayamdost, M. R. Antibiotic dialogues: induction of silent biosynthetic gene clusters by exogenous small molecules. *FEMS Microbiol. Rev.* **41**, 19–33 (2017).
11. Ochi, K. & Hosaka, T. New strategies for drug discovery: activation of silent or weakly expressed microbial gene clusters. *Appl. Microbiol. Biotechnol.* **97**, 87–98 (2013).
12. Rutledge, P. J. & Challis, G. L. Discovery of microbial natural products by activation of silent biosynthetic gene clusters. *Nat. Rev. Microbiol.* **13**, 509–523 (2015).
13. Zhu, H., Sandiford, S. K. & van Wezel, G. P. Triggers and cues that activate antibiotic production by actinomycetes. *J. Ind. Microbiol. Biotechnol.* **41**, 371–386 (2014).
14. Nah, H. J., Pyeon, H. R., Kang, S. H., Choi, S. S. & Kim, E. S. Cloning and heterologous expression of a large-sized natural product biosynthetic gene cluster in streptomyces species. *Front. Microbiol.* **8**, 394 (2017).
15. Ren, H., Wang, B. & Zhao, H. Breaking the silence: new strategies for discovering novel natural products. *Curr. Opin. Biotechnol.* **48**, 21–27 (2017).
16. Yoon, V. & Nodwell, J. R. Activating secondary metabolism with stress and chemicals. *J. Ind. Microbiol. Biotechnol.* **41**, 415–424 (2014).
17. Guo, F. et al. Targeted activation of silent natural product biosynthesis pathways by reporter-guided mutant selection. *Metab. Eng.* **28**, 134–142 (2015).
18. Seyedsayamdost, M. R. High-throughput platform for the discovery of elicitors of silent bacterial gene clusters. *Proc. Natl Acad. Sci. USA* **111**, 7266–7271 (2014).
19. Xu, F., Nazari, B., Moon, K., Bushin, L. B. & Seyedsayamdost, M. R. Discovery of a cryptic antifungal compound from *Streptomyces albus* J1074 using high-throughput elicitor screens. *J. Am. Chem. Soc.* **139**, 9203–9212 (2017).
20. Rosen, P. C. & Seyedsayamdost, M. R. Though much is taken, much abides: finding new antibiotics using old ones. *Biochemistry* **56**, 4925–4926 (2017).
21. Watrous, J. D. & Dorrestein, P. C. Imaging mass spectrometry in microbiology. *Nat. Rev. Microbiol.* **9**, 683–694 (2011).
22. Gross, H. et al. The genomisotopic approach: a systematic method to isolate products of orphan biosynthetic gene clusters. *Chem. Biol.* **14**, 53–63 (2007).
23. Nemes, P. & Vertes, A. Laser ablation electrospray ionization for atmospheric pressure, in vivo, and imaging mass spectrometry. *Anal. Chem.* **79**, 8098–8106 (2007).
24. Li, H., Balan, P. & Vertes, A. Molecular imaging of growth, metabolism, and antibiotic inhibition in bacterial colonies by laser ablation electrospray ionization mass spectrometry. *Angew. Chem. Int. Edn Engl.* **55**, 15035–15039 (2016).
25. Fincher, J. A. et al. Enhanced sensitivity and metabolite coverage with remote laser ablation electrospray ionization-mass spectrometry aided by coaxial plume and gas dynamics. *Analyst* **142**, 3157–3164 (2017).
26. Li, H. & Vertes, A. Solvent gradient electrospray for laser ablation electrospray ionization mass spectrometry. *Analyst* **142**, 2921–2927 (2017).
27. Heinemann, B., Kaplan, M. A., Muir, R. D. & Hooper, I. R. Amphomycin, a new antibiotic. *Antibiot. Chemother. (Northfield)* **3**, 1239–1242 (1953).
28. Bodanszky, M., Sigler, G. F. & Bodanszky, A. Structure of the peptide antibiotic amphomycin. *J. Am. Chem. Soc.* **95**, 2352–2357 (1973).
29. Maksimov, M. O., Pan, S. J. & Link, A.J. Lasso peptides: structure, function, biosynthesis, and engineering. *Nat. Prod. Rep.* **29**, 996–1006 (2012).
30. Hegemann, J. D., Zimmermann, M., Xie, X. & Marahiel, M. A. Lasso peptides: an intriguing class of bacterial natural products. *Acc. Chem. Res.* **48**, 1909–1919 (2015).
31. Güntert, P., Mumenthaler, C. & Wüthrich, K. Torsion angle dynamics for NMR structure calculation with the new program DYANA. *J. Mol. Biol.* **273**, 283–298 (1997).
32. Herrmann, T., Güntert, P. & Wüthrich, K. Protein NMR structure determination with automated NOE-identification in the NOESY spectra using the new software ATNOS. *J. Biomol. NMR* **24**, 171–189 (2002).
33. Zhu, S. et al. Insights into the unique phosphorylation of the lasso peptide paeninodin. *J. Biol. Chem.* **291**, 13662–13678 (2016).
34. Tietz, J. I. et al. A new genome-mining tool redefines the lasso peptide biosynthetic landscape. *Nat. Chem. Biol.* **13**, 470–478 (2017).
35. Price, J. C., Barr, E. W., Tirupati, B., Bollinger, J. M. Jr. & Krebs, C. The first direct characterization of a high-valent iron intermediate in the reaction of an α-ketoglutarate-dependent dioxygenase: a high-spin Fe^{IV} complex in taurine/α-ketoglutarate dioxygenase (TauD) from *Escherichia coli*. *Biochemistry* **42**, 7497–7508 (2003).
36. Krebs, C., Galonić Fujimori, D., Walsh, C. T. & Bollinger, J. M. Jr. Non-heme Fe(IV)-oxo intermediates. *Acc. Chem. Res.* **40**, 484–492 (2007).
37. Tiwari, K. & Gupta, R. K. Rare actinomycetes: a potential storehouse for novel antibiotics. *Crit. Rev. Biotechnol.* **32**, 108–132 (2012).
38. Nicolaou, K. C., Boddy, C. N., Bräse, S. & Winssinger, N. Chemistry, biology, and medicine of the glycopeptide antibiotics. *Angew. Chem. Int. Edn Engl.* **38**, 2096–2152 (1999).
39. Hubbard, B. K. & Walsh, C. T. Vancomycin assembly: nature's way. *Angew. Chem. Int. Edn Engl.* **42**, 730–765 (2003).
40. Shen, B., Liu, W. & Nonaka, K. Enediyne natural products: biosynthesis and prospect towards engineering novel antitumor agents. *Curr. Med. Chem.* **10**, 2317–2325 (2003).

41. Everest, G. J. & Meyers, P. R. Evaluation of the antibiotic biosynthetic potential of the genus *Amycolatopsis* and description of *Amycolatopsis circi* sp. nov., *Amycolatopsis equina* sp. nov. and *Amycolatopsis hippodromi* sp. nov. *J. Appl. Microbiol.* **111**, 300–311 (2011).
42. Heald, S. L., Mueller, L. & Jeffs, P. W. Actinoidins A and A2: structure determination using 2D NMR methods. *J. Antibiot. (Tokyo)* **40**, 630–645 (1987).
43. Berdnikova, T. F., Lomakina, N. N. & Potapova, N. P. [Structure of actinoidins A and B]. *Antibiotiki* **27**, 252–258 (1982).
44. Diekema, D. J. & Jones, R. N. Oxazolidinone antibiotics. *Lancet* **358**, 1975–1982 (2001).
45. Jorquera, P. A. & Tripp, R. A. Respiratory syncytial virus: prospects for new and emerging therapeutics. *Expert Rev. Respir. Med.* **11**, 609–615 (2017).
46. Yang, Y. L., Xu, Y., Straight, P. & Dorrestein, P. C. Translating metabolic exchange with imaging mass spectrometry. *Nat. Chem. Biol.* **5**, 885–887 (2009).
47. Kersten, R. D. et al. A mass spectrometry-guided genome mining approach for natural product peptidogenomics. *Nat. Chem. Biol.* **7**, 794–802 (2011).
48. Traxler, M. F., Watrous, J. D., Alexandrov, T., Dorrestein, P. C. & Kolter, R. Interspecies interactions stimulate diversification of the *Streptomyces coelicolor* secreted metabolome. *mBio* **4**, e00459–13 (2013).
49. Du, L. et al. Unique amalgamation of primary and secondary structural elements transform peptaibols into potent bioactive cell-penetrating peptides. *Proc. Natl Acad. Sci. USA* **114**, E8957–E8966 (2017).
50. Craney, A., Ozimok, C., Pimentel-Elardo, S. M., Capretta, A. & Nodwell, J. R. Chemical perturbation of secondary metabolism demonstrates important links to primary metabolism. *Chem. Biol.* **19**, 1020–1027 (2012).
51. Goodwin, C. R. et al. Structuring microbial metabolic responses to multiplexed stimuli via self-organizing metabolomics maps. *Chem. Biol.* **22**, 661–670 (2015).
52. Okada, B. K., Wu, Y., Mao, D., Bushin, L. B. & Seyedsayamdost, M. R. Mapping the trimethoprim-induced secondary metabolome of *Burkholderia thailandensis*. *ACS Chem. Biol.* **11**, 2124–2130 (2016).
53. Davies, J., Spiegelman, G. B. & Yim, G. The world of subinhibitory antibiotic concentrations. *Curr. Opin. Microbiol.* **9**, 445–453 (2006).
54. Yim, G., Wang, H. H. & Davies, J. Antibiotics as signalling molecules. *Phil. Trans. R. Soc. Lond. B* **362**, 1195–1200 (2007).
55. Romero, D., Traxler, M. F., López, D. & Kolter, R. Antibiotics as signal molecules. *Chem. Rev.* **111**, 5492–5505 (2011).

Acknowledgements

We thank the National Institutes of Health (DP2-AI-124786 to M.R.S.), the Burroughs Wellcome Fund, and the Princeton IP Accelerator Fund for support of this work. K.M.D. was supported by an Arnold O. Beckman Postdoctoral Fellowship. L.B.B. was supported by a National Science Foundation Graduate Research Fellowship.

Author contributions

F.X., Y.W., and M.R.S. designed the research; F.X., Y.W., and C.Z. carried out high-throughput elicitor screens and validations; Y.W. conducted the LAESI–IMS experiments and analyzed the results; F.X. purified and solved the structures of all secondary metabolites, with assistance from K.M.D. and K.M. Y.W. conducted structure calculations, with assistance from L.B.B. F.X. carried out bioinformatic analyses. M.R.S. wrote the manuscript, to which all authors contributed. F.X. and Y.W. contributed equally to this work.

Competing interests

The authors declare no competing interests.

Additional information

Supplementary information is available for this paper at https://doi.org/10.1038/s41589-018-0193-2.

Reprints and permissions information is available at www.nature.com/reprints.

Correspondence and requests for materials should be addressed to M.R.S.

Publisher's note: Springer Nature remains neutral with regard to jurisdictional claims in published maps and institutional affiliations.

Methods

Bacterial strains and culture media. *P. protegens* Pf-5 was obtained from the ATCC. *A. keratiniphila* subsp. *keratiniphila* NRRL B-24117 and *S. canus* NRRL B-3980 were acquired from the ARS (NRRL) culture collection. All culture media were obtained from Becton-Dickinson. Other media components were obtained from Sigma-Aldrich.

Screens of *P. protegens* Pf-5. *P. protegens* was streaked out onto an LB-agar plate from frozen culture stocks and grown at 30 °C overnight. Colonies were used to inoculate 5 mL of LB in a 14-mL sterile culture tube, which was cultured for 12–13 h at 30 °C/250 r.p.m. The overnight culture was then used to inoculate 550 mL LB in a sterile Erlenmeyer flask to an initial optical density at 600 nm of 0.01. The culture was distributed into six sterile, deep-well 96-well plates (0.9 mL per well) with a MultiFlo Microplate Dispenser (BioTek). Subsequently, elicitors were added from a commercially available 502-member natural-product library (Enzo Scientific, BML-2865) with a CyBi-Well automated liquid transfer robot (CyBio). Each well received 2.5 µL of an elicitor (from a stock concentration of 2 mg/mL). The plates were sealed with air-permeable membranes and grown at 25 °C/200 r.p.m. After 44 h, the plates were spun down, supernatants were loaded onto a 96-well Strata C8-resin plate (Phenomenex), and the material was eluted with 600 µL of 50% and 600 µL 100% MeCN into fresh 96 well plates. The eluates were dried in a SpeedVac concentrator, resuspended in 30 µL of 40% MeCN (in water), and imaged with LAESI–MS (described below).

Screens of *S. canus* and *A. keratiniphila*. Freshly collected spores of *S. canus* or *A. keratiniphila* (~10^7) were transferred to 50 mL YEME medium (0.3% (wt/vol) yeast extract, 0.5% peptone, 0.3% malt extract, 1% glucose, 34% sucrose, and 5 mM $MgCl_2 \bullet 6H_2O$) in a 250-mL Erlenmeyer flask fitted with a stainless-steel spring and cultured at 30 °C/250 r.p.m. for 3 d. Mycelia were then collected by centrifugation (10 min, 3,000*g*, RT) and diluted into 300 mL of R4 medium, to a final concentration of 0.05% (wt/vol). R4 medium consisted of 0.5% (wt/vol) glucose, 0.1% yeast extract, 0.5% $MgCl_2 \bullet 6H_2O$, 0.2% $CaCl_2 \bullet 2H_2O$, 0.15% proline, 0.118% valine, 0.28% TES, 50 mg/L-casamino acids, 100 mg/L K_2SO_4, and 1× trace-element solution (40 mg/L $ZnCl_2$, 200 mg/L $FeCl_3 \bullet 6H_2O$, 10 mg/L $CuCl_2 \bullet 2H_2O$, 10 mg/L $MnCl_2 \bullet 4H_2O$, 10 mg/L $Na_2B_4O_7 \bullet 10H_2O$, and 10 mg/L $(NH_4)_6Mo_7O_24 \bullet 4H_2O$)[56]. Subsequently 300 µL was dispensed into six deep-well 96-well plates with a MultiFlo Microplate Dispenser. The wells were supplemented with candidate elicitors from the same 502-member natural-product library used above with the aid of a CyBi-Well automated liquid transfer robot. Each well received 0.85 µL of an elicitor (from a stock concentration of 2 mg/mL). The plates were sealed with air-permeable membranes and grown at 30 °C/250 r.p.m. After 5 d, the samples were desalted as described above for *P. protegens* and imaged with LAESI–IMS (described below).

Analysis by LAESI–IMS. A LAESI DP1000 system (Protea Bioscience) coupled to an LTQ XL mass spectrometer (Thermo) was used for IMS analysis. The extension tube connecting the two instruments was kept at 130 °C with an external heater, and the sample stage was kept at 10 °C during analysis. The sheath-gas flow was set to 2.0 L/h. Eighty laser pulses were applied to each well to ablate samples with an 80% laser energy setting (~850 µJ) and a 10-Hz frequency. A solution of 2:1 MeCN/water with 0.1% acetic acid (vol/vol) was supplied as the electrospray solution with a syringe pump running at a flow rate of 1 µL/min. We found this solution to be effective in the detection of a variety of structurally distinct metabolites, including alkaloids, quinolones, small aromatic compounds, GPAs, and other peptides. The emitter was connected to high-voltage power operating at +4,000 V or +4,500 V in positive-ion detection mode. All data were visualized in ProteaPlot software.

After data collection, the signals observed in each well were extracted with GMSU-LAESI software (Gubbs), which yielded all m/z values and the corresponding intensities per well (i.e., per elicitor). The data were binned in 1-m/z units for 3D plotting. Signals with an intensity value lower than a set threshold were not included in the 3D plots. The data were plotted in MatLab with the bar3 function. Simple visual inspection of 3D plots generated in this fashion allowed us to identify metabolites whose production was induced or enhanced by a given elicitor. Because low-MW metabolites generally ionized better than high-MW compounds, a higher threshold was used for visualizing the former (intensity scale bars in 3D plot figures).

The 3D plot provides a visual readout of the effects of all small molecules in the library on all MS-detected secondary metabolites. The effect of the small molecules in the library on the production of a single metabolite was best assessed in the component 2D plots (Figs. 3b and 4b). The component 2D plots were extracted from the corresponding 3D data in MatLab and plotted in Excel. The 2D plots were normalized to the highest-intensity peak. Hits identified in this manner were validated with flask cultures and HPLC–MS analysis, as described below. Elicitation of orfamides, canucins, keratinimicins, and keratinicyclins was also observed in large-scale cultures. It is possible that the production of some compounds may not translate well from 96-well plates to flask cultures, although this was not the case with the compounds that we pursued.

Validation of HiTES elicitors. To validate the induction of the cryptic metabolite identified in the high-throughput screen, we grew flask cultures of each condition and analyzed them by HPLC–MS. To validate orfamide production, we prepared 5-mL overnight cultures of *P. protegens* as described above. The culture was then diluted into two 125-mL Erlenmeyer flasks, each containing 20 mL of LB to an initial optical density at 600 nm of 0.01. One flask was supplemented with cafestol (22 µM final concentration), and the other was supplemented with the same volume of DMSO (control). Both cultures were incubated at 25 °C/150 r.p.m. After 44 h, the cells were removed by centrifugation, and 10 mL of each supernatant was desalted on a C8 PrepSep solid-phase extraction column (Fisher). After loading, the columns were washed with H_2O, and bound material was eluted with a two-step gradient of 50% MeCN (in H_2O) and 100% MeCN. The fractions were dried in vacuo, redissolved in 100 µL MeOH, and analyzed with HPLC-Qtof-MS (described below).

To validate canucin production, we prepared seed cultures of *S. canus* as described above. The culture was diluted into two 250-mL Erlenmeyer flasks, each containing 50 mL of R4 medium to a final mycelial concentration of 0.05% (wt/vol). Kenpaullone was added to one flask (final concentration of 17 µM), and the other flask served as a control and received the same volume of DMSO. The cultures were grown at 30 °C/200 r.p.m. for 5 d. The supernatants were extracted twice with 30 mL of ethyl acetate. The organic phases were combined, dried in vacuo, redissolved in 200 µL MeOH, and analyzed with HPLC-Qtof-MS (described below).

To validate keratinimicin and keratinicyclin production, we prepared seed cultures of *A. keratiniphila* as above. The cultures were diluted into three 1-mL wells in a deep 96-well plate containing 0.9 mL of R4 medium at a final mycelial concentration of 0.05% (wt/vol). The 96-well plate was supplemented with a final concentration of 7.8 µM vincamine (well 1), 2 µM Dhe (well 2), and the same volume of DMSO (well 3, control). The plate was then grown at 30 °C/200 r.p.m. for 5 d. Cells and mycelia were removed by centrifugation, and the wells were worked up as noted above for the 96-well screens and analyzed with HPLC-Qtof-MS. Alternatively, the seed culture was diluted into three 250-mL Erlenmeyer flasks carrying 50 mL of R4 medium at a mycelial concentration of 0.05% (wt/vol). The flasks were supplemented with 7.8 µM Vin (flask 1), 2 µM Dhe (flask 2), or the same volume of DMSO (flask 3, control), then grown at 30 °C/200 r.p.m. for 5 d. Cells and mycelia were removed, and 10 mL of each supernatant was loaded onto a C18 SPE column (Phenomenex, 100 mg), washed with H_2O, and eluted with 50% and 100% MeCN. The fractions were dried in vacuo, redissolved in 100 µL MeOH, and analyzed with HPLC-Qtof-MS. The deep-well-plate method resulted in better induction of keratinimicin and keratinicyclin. All validations were carried out in three independent biological replicates.

HPLC–MS and HPLC analysis. HPLC–MS analysis was performed on an Agilent 1260 Infinity Series HPLC system equipped with an automated liquid sampler, a diode array detector, and a 6120 Series ESI mass spectrometer with a reversed-phase Luna C18 column (Phenomenex, 5 µm, 150 × 4.6 mm). The mobile phases consisted of H_2O and MeCN (+0.1% formic acid). Elution was carried out isocratically with 5% MeCN in water for 3 min, followed by gradients of 5–70% MeCN over 20 min, then 70–100% over 5 min, at a flow rate of 0.6 mL/min. High-resolution (HR) HPLC–MS and HR tandem HPLC–MS were carried out on an Agilent 6540 Accurate Mass Qtof LC-MS, consisting of a 1260 Infinity Series HPLC system, an automated liquid sampler, a diode array detector, a JetStream ESI source, and the 6540 Series Qtof. Samples were resolved on a Luna C18 column (Phenomenex, 5 µm, 100 × 4.6 mm). The mobile phase consisted of water and MeCN (+0.1% formic acid). Elution for orfamides was carried out isocratically with 10% MeCN in water (3 min) followed by a gradient of 10–95% MeCN over 8 min, and an isocratic elution at 95% MeCN over 25 min at a flow rate of 0.4 mL/min. Elution of canucins, keratinimicins, and kertinicyclins was carried out isocratically with 5% MeCN in water (3 min) followed by a gradient of 5–95% MeCN in water over 15 min, at a flow rate of 0.4 mL/min.

HPLC purifications were carried out on an Agilent preparative HPLC system equipped with a 1260 Infinity series binary pump, a diode array detector, and an automated fraction collector. Semipreparative or analytical-scale purifications were performed on an Agilent HPLC system containing a 1260 Infinity Series binary pump or a 1290 Infinity quaternary pump. Each system was equipped with an automatic liquid sampler, a temperature-controlled column compartment, a diode array detector, and an automated fraction collector.

Large-scale growth of *S. canus* and *A. keratiniphila*. Large-scale fermentation was carried out through a similar procedure to that for the small-scale fermentations described above. Three-day seed cultures were prepared as above, and mycelia were isolated and used to inoculate several 2-L Erlenmeyer flasks containing 200 mL of R4 medium to a final mycelial concentration of 0.01% (wt/vol). The culture was then supplemented with the optimal concentration of the elicitor (described above). Typically, 8–12 L of total culture was used for compound isolation. The flasks were incubated at 30 °C/250 r.p.m. for 7 d, at which point the desired products were purified (described below).

Purification of canucin A and B. Canucins were purified from 12-L fermentation of *S. canus* in the presence of kenpaullone (at a final concentration of 17 µM). After a 7-day fermentation, the supernatant was extracted twice with an equal volume

of ethyl acetate. The combined organic phase was dried over Na_2SO_4 in vacuo, resuspended in 45 mL MeOH, and purified on an Agilent Preparative HPLC. The sample was resolved with repeated injections onto a preparative Luna C18 column (Phenomenex, 5 µm, 21.2 × 250 mm) operating at a flow rate of 12 mL/min with mobile phases consisting of water and MeCN (+0.1% formic acid). After injection, elution was carried out isocratically with 20% MeCN for 2 min, followed by a gradient of 20–100% MeCN over 25 min. Peaks containing canucin A and B, as judged by HPLC–MS, were pooled, dried in vacuo, resuspended in MeOH, and further purified on a semipreparative/analytical HPLC system. The peptides were resolved on a semipreparative XDB-C8 column (Agilent, 5 µm, 10 × 250 mm) operating at a flow rate of 2.5 mL/min with a gradient of 30–50% MeCN (in water) over 30 min, followed by a gradient of 50–100% MeCN over 5 min. Peaks containing pure canucin B were combined and lyophilized to dryness. Peaks containing canucin A were pooled, dried in vacuo, resuspended in MeOH, and further purified on a semipreparative Luna C18 column (Phenomenex, 5 µm, 10 × 250 mm) with a gradient of 33–55% MeCN over 30 min, followed by a gradient of 55–100% MeCN over 5 min. Peaks containing pure canucin A were combined and lyophilized to dryness. This procedure yielded 3.6 mg of canucin A and 1.7 mg canucin B.

Purification of keratinimicins and keratinicyclins. Keratinimicins and keratinicyclins were purified from 8-L fermentations of *A. keratiniphila* in the presence of 2 µM Dhe. After a 7-d fermentation, the resulting supernatant was loaded on a prepacked C18 column (Phenomenex, 50 µm, 65 Å, 10 g) and eluted with 20%, 50%, and 100% MeCN in water stepwise. The 20% fraction containing keratinimicins and keratinicyclins was dried in vacuo, resuspended in 50 mL MeOH, and further purified by preparative HPLC with a Luna C18 column (Phenomenex, 5 µm, 21.2 × 250 mm) operating at a flow rate of 12 mL/min with mobile phases consisting of water and MeCN (+0.1% formic acid). After injection, elution was carried out isocratically with 5% MeCN in water for 2 min, followed by a gradient of 5–40% MeCN in water over 20 min, and a gradient of 40–100% MeCN over 5 min. Fractions were collected in 1-min intervals over the time range of 5–25 min. Peaks containing keratinimicin A-D, as judged by HPLC–MS analysis, were pooled, dried in vacuo, resuspended in MeOH and further purified on a semipreparative/analytical HPLC system. The sample was applied to a an RP amide-C16 column (Supelco, 5 µm, 10 × 250 mm) operating at a flow rate of 2.5 mL/min with the same mobile phases as above and a gradient of 8–16% MeCN in water over 30 min, followed by a gradient of 16–100% MeCN over 5 min. Peaks containing pure keratinimicin C and D were combined and lyophilized to dryness. Peaks containing keratinimicin A and B were pooled, dried in vacuo, resuspended in MeOH and further purified on a semipreparative XDB-C8 column (Agilent, 5 µm, 10 × 250 mm) with a gradient of 5–15% MeCN in water over 30 min, followed by a gradient of 15–100% MeCN over 5 min. Peaks containing pure keratinimicin A and B were combined and lyophilized to dryness. This procedure yielded 8.5 mg of keratinimicin A, 1.6 mg keratinimicin B, 5.1 mg keratinimicin C, and 0.8 mg keratinimicin D.

Peaks containing keratinicyclin A–C from the preparative Luna C18 column were pooled, dried in vacuo, resuspended in MeOH and further purified on a semipreparative/analytical HPLC system. The sample was applied to an RP amide-C16 column (Supelco, 5 µm, 10 × 250 mm) operating at a flow rate of 2.5 mL/min with the same mobile phase as above and a gradient of 10–20% MeCN in water over 30 min, followed by a gradient of 20–100% MeCN over 5 min. Peaks containing pure keratinicyclin A and C were combined and lyophilized to dryness. Peaks containing keratinicyclin B were pooled, dried in vacuo, resuspended in MeOH and further purified on a semipreparative XDB-C8 column (Agilent, 5 µm, 10 × 250 mm) with a gradient of 5–15% MeCN in water over 30 min, followed by a gradient of 15–100% MeCN over 5 min. This procedure yielded 2.7 mg of keratinicyclin A, 5.3 mg keratinicyclin B, and 1.2 mg keratinicyclin C.

Structural elucidation of canucins, keratinimicins, and keratinicyclins. HR–MS data for all compounds and their inferred molecular formula are listed in Supplementary Table 1. For structural elucidation, 1D/2D NMR spectra were acquired at the Princeton University Department of Chemistry NMR Facilities on an A8 Avance III HD 800-MHz NMR spectrometer (Bruker) with a triple-resonance cryoprobe. The NMR samples of keratinimicin A–D and keratinicyclin A–C were prepared in DMSO-*d6*, and those of canucin A and B were prepared in CD_3OH. 1D/2D NMR spectra of canucin A, keratinimicin A, and keratinicyclin A are shown (Supplementary Figs. 3, 5 and 6). NMR tables listing chemical-shift assignments for all compounds can be found in Supplementary Tables 2, 4, 6, and 8–13.

3D structure calculations of canucins. A NOESY spectrum of canucin A acquired in CD_3OH at 295 K with a mixing time of 500 ms exhibited the greatest number of correlations while avoiding spin diffusion, and was therefore used for structure calculations. Cross-peak positions and volumes in this spectrum were measured in MestReNova and assigned manually. These were given as initial input data for the calculations, which were performed in CYANA 2.1 on a Linux cluster. The isopeptide bond was incorporated via explicit distance constraints for the N–C bond between the N of Gly1 and the C_γ of Asp8. Specifically, both upper and lower limits for the N–C_γ bond length were set to 1.4 Å, with weighting factors of 1.00. These distances were based on the average bond length of an amide bond. The unnatural amino acid β-OH-aspartate in canucin A was encoded into the CYANA residue library with CYLIB software[57]. Seven cycles of combined NOESY assignment and structure calculation were performed, and this was followed by a final structure calculation. Calibration parameters for the extraction of distance constraints from cross-peak volumes were determined automatically. For each cycle and for the final calculation, 100 initial conformers were generated, and a simulated annealing schedule, composed of 10,000 torsion-angle dynamic steps, was applied to each conformer. We generated statistics for the ten conformers with the lowest final target functions (Supplementary Table 3). The calculated conformers were visualized in PyMOL.

Assignment of the locations of sugars on keratinimicin A. The locations of mono- and disaccharide substituents was assigned on the basis of 1D/2D NMR spectra: sugar Cg (Supplementary Table 6) was easily assigned by observation of HMBC correlations between Cg1 and Cβ of the amino acid residue (residue C). Specifically, two key HMBC correlations were observed: Cg1-^{1}H at 4.67 p.p.m. correlated with Cβ at 74.8 p.p.m.; and Cβ1-^{1}H at 5.11 p.p.m. correlated with Cg1 at 94.2 p.p.m.).

For sugars Dg and Dg', we first confirmed the assignments of the amino acids in the peptide scaffold and subsequently assigned the sugar signals. Two signals with shifts at 5.17 and 5.65 p.p.m. were assigned as side chain ^{1}Hs on residue D. These showed HMBC correlations to the α-carbon of residue D at 54.6 p.p.m. as well as an aromatic carbon at 132.4 p.p.m. (C4, residue D), in addition to three-bond correlations to the opposing C2 (104.9 p.p.m.) and C6 (108.4 p.p.m.). They also weakly interacted with each other, as is characteristic of a W-coupling interaction. ROSEY interactions from these protons (i.e., to the C3-^{1}H and C5-^{1}H on residue E at 7.22 and 7.13 p.p.m., respectively) were all consistent with the assignment of these signals as ^{1}Hs on the residue-D side chain. A signal (δ H/δC, 5.67/99.8) was found to correlate with C4 on residue D (132.4 p.p.m.). Additional COSY and HMBC correlations from this signal were consistent with its assignment as the anomeric position on sugar Dg. This C1-^{1}H on sugar Dg was found to correlate to another spin system via HMBC, specifically a signal with an δH/δC of 5.18/100.6 p.p.m. This signal was assigned to the anomeric position on sugar Dg', an assignment consistent with the COSY and HMBC data on this Dg spin system.

After assignment of two of the three overlapping signals (δH/δC, 5.17/104.9 and 5.18/100.6), the remaining one (5.18/98.1 p.p.m.) was assigned to the anomeric position on sugar Ag, which was consistent among others with an HMBC correlation from C1-^{1}H on Ag to C5 (155.2 p.p.m.) on the residue-A side chain. A similar process was used to assign the location of sugars in keratinimicin B–D.

Assignment of β-OH stereochemistry in keratinimicin A. To assign the β-OH stereocenter in keratinimicin A, we noted the NOE correlations from the β-^{1}H of residue C (5.11 p.p.m.) to the α-^{1}H (4.23 p.p.m.) and aromatic C2-^{1}H (7.89 p.p.m.) on residue C, but not to the aromatic C6-^{1}H (7.36 p.p.m.), thus indicating that the Cα-^{1}H, Cβ-^{1}H, and C2-^{1}H were close in space. The α-carbon is in the *S* configuration, as deduced from NRPS domain analysis of the *ker* gene cluster. This information together led us to propose the *R* configuration for the β-^{1}H on residue C. A similar analysis was conducted with residue E: the β-^{1}H (5.20 p.p.m.) showed a strong NOE with the α-^{1}H (4.52 p.p.m.) and the aromatic C6-^{1}H (7.05 p.p.m.), but not the C2-^{1}H (7.78 p.p.m.), thus suggesting that the α-^{1}H, Cβ-^{1}H, and C6-^{1}H were close in space. Given the *R* configuration of the α-carbon on residue E, we predicted the *R* configuration for its β-carbon.

Genomic-DNA isolation and sequencing. *A. keratiniphila* was cultured in 25 mL YEME medium for 2 d, and the mycelium was subsequently harvested to isolate the genomic DNA with a Promega Wizard Genomic DNA Purification Kit, per the manufacturer's instructions. Genomic DNA of high quality was obtained at a concentration of 990 ng/µL and a $UV_{260/280}$ value of 1.8.

To sequence the *ker* gene cluster, we submitted genomic DNA to the Lewis Sigler Institute Sequencing Core Facility, where short-DNA-fragment libraries were prepared via an Illumina MiSeq Reagent Kit, and the fragments were sequenced on an Illumina MiSeq System. The raw sequence data were assembled with Unicycler and SPAdes software. A total of 229 contigs covering 9.1 Mbp were obtained. Genome annotation was carried out via the RAST server 2.0. The data were then searched with the OxyB sequence from *Amycolatopsis orientalis* as a query, thus allowing us to identify the *ker* cluster. By examining the sequence 75 kb upstream and downstream of the OxyB homolog, we were able to assign the cluster boundaries. Predicted protein functions were assigned with the IMG and antiSMASH databases. The sequence for the entire *ker* gene cluster was uploaded to NCBI (accession no. MH428036).

Antibacterial and antiviral assays. Antibacterial assays were carried out by Micromyx, in accordance with methods from the Clinical and Laboratory Standards Institute. Minimal inhibitory concentrations were determined with the following strains (listed in Table 1 and Supplementary Table 14): *Staphylococcus aureus* ATCC 29213, *S. aureus* MMX 2011, *Streptococcus pneumoniae* ATCC

49619, *Streptococcus pyogenes* MMX 6253, *Streptococcus agalactiae* MMX 6189, *E. faecalis* ATCC 29212, *E. faecalis* MMX 486, *Bacillus subtilis* ATCC 6633, *Escherichia coli* ATCC 25922, *K. pneumoniae* MMX 214, *P. aeruginosa* ATCC 27853, *A. baumannii* ATCC 19606, *V. cholerae* BAA-2163, *C. difficile* ATCC 700057, and *Bacteroides fragilis* ATCC 25285.

Antiviral assays were performed by Virapur in accordance with methods from the Clinical and Laboratory Standards Institute. Minimal inhibitory concentrations were determined with the following viruses and host cells (listed in Table 1 and Supplementary Table 14): influenza A/Perth/16/2009 in MDCK cells, influenza B/Wisconsin/1/2010 in MDCK cells, herpes simplex 1 strain MacIntyre in Vero cells, herpes simplex 2 strain G in Vero cells, vaccinia virus WR in Vero cells, rhinovirus 8 in HeLa cells, and RSV in Hep2 cells.

All assays (antibacterial and antiviral) were carried out in triplicate and yielded identical MIC values for all replicates (Table 1). As such, ranges or errors were not available to report.

Statistics and reproducibility. All HiTES–IMS screens (Figs. 2a, 3a and 4a and Supplementary Figs. 2 and 4) were carried out in a single replicate; production of the desired cryptic metabolites was validated in three independent biological replicates (Figs. 2c, 3c and 4b). All replicates yielded similar levels of induction of orfamides, canucins, keratinimicins, and keratinicyclins with the respective elicitors. Figures 3b and 4b are 2D slices from the 3D plots in Figs. 3a and 4a, respectively. Full 1D/2D NMR datasets for canucins, keratinimicins, and keratinicyclins (Supplementary Figs. 3, 5, and 6 and Supplementary Tables 2, 4, 6, and 8–13) were collected once. Antibacterial and antiviral MIC measurements were carried out in three independent replicates, and identical MIC values were obtained in all cases; these are listed in Table 1 and Supplementary Table 14.

Reporting Summary. Further information on research design is available in the Nature Research Reporting Summary linked to this article.

Data availability

The data supporting the findings of this study are available within the paper and the supplementary material. NMR data used to characterize the cryptic metabolites are available from the corresponding author upon reasonable request. The DNA sequence of the *ker* gene cluster from *A. keratiniphila* has been deposited in GenBank (accession no. MH428036). The LAESI–IMS data for *S. canus* and *A. keratiniphila*, including the raw data for Figs. 3a and 4a as well as the source code used to generate the 3D plots, have been deposited in the Global Natural Products Social Molecular Networking (GNPS) database (MassIVE accession number MSV000082658).

References

56. Hu, H. & Ochi, K. Novel approach for improving the productivity of antibiotic-producing strains by inducing combined resistant mutations. *Appl. Environ. Microbiol.* **67**, 1885–1892 (2001).
57. Yilmaz, E. M. & Güntert, P. NMR structure calculation for all small molecule ligands and non-standard residues from the PDB Chemical Component Dictionary. *J. Biomol. NMR* **63**, 21–37 (2015).